

Label-free continuous cell sorter with specifically adhesive oblique micro-grooves

Takahiro Nishimura, Junichi Miwa¹, Yuji Suzuki and Nobuhide Kasagi

Department of Mechanical Engineering, The University of Tokyo, Hongo 7-3-1, Bunkyo-ku, Tokyo 113-8656, Japan

E-mail: miwa@thtlab.t.u-tokyo.ac.jp

Received 14 April 2009, in final form 3 September 2009

Published 20 October 2009

Online at stacks.iop.org/JMM/19/125002

Abstract

We report the development of a label-free continuous cell sorting method based on specific adhesivity between cells and surface-immobilized adhesion molecules. The separation of cells is induced by cross-flow adhesive force on micron-sized stripes with adhesion molecules immobilized on the surface. In order to accurately form the adhesive stripes on a microchannel wall, 1 μm wide micro-grooves are fabricated at a certain angle with respect to the flow direction using direct electron-beam lithography. Amino-functionalized parylene is used as the groove surface material, and streptavidin is immobilized on the entire surface, resulting in a surface with periodic adhesive patterns. The effectiveness of the proposed cell sorting principle is verified by flow-through experiments using functionalized particles as model cells. Measurements of the motion of biotin-coated microparticles show that the particles decelerated by specific adhesivity are displaced in the cross-flow direction. The observed cross-flow displacement is around 0.8% of the streamwise travelling distance. It is also shown that the rate of cross-flow displacement is independent of the flow rate or the stripe angle. Finally, it is demonstrated that a mixture of streptavidin- and biotin-coated microparticles can be completely separated after flowing over a 20 mm long patterned surface. The proposed label-free continuous lateral separation scheme has a wide range of potential applications for separation of cells which could not be distinguished by size or separated using dielectric forces.

(Some figures in this article are in colour only in the electronic version)

1. Introduction

Stem cell therapy is a rapidly evolving biomedical technology, in which multipotent stem cells are cultured *in vitro* and transplanted to regenerate damaged or deficit tissue. The major candidate cell for use in stem cell therapy is currently the embryonic stem cell [1] or the recently proposed induced pluripotent stem cell [2], both of them promising in terms of their abilities to differentiate into various cell types. On the other hand, some adult stem cells such as the mesenchymal stem cell (MSC) also show the ability to differentiate into

various tissue cells [3]. Because MSC can be found in human bone marrow or peripheral blood [4, 5], there are no ethical problems in using the cells, and no additional steps such as virus vector introduction are required. However, the number of MSC is only around 10^{-8} of all mononuclear cells even in umbilical cord blood [4], which gives rise to the need of an efficient and accurate cell separation method for stem cell extraction from patients' bodies. The conventional method for MSC isolation from blood involves density-gradient centrifugation and subsequent cell culture [4, 5], the latter of which can take several weeks. On the other hand, the present state-of-the-art technology in regenerative medicine also enables a small amount of stem cells to be directly transplanted to the organ in concern, to replace the damaged part of the body [6]. Therefore, an efficient cell

¹ Present address: Laboratory for MEMS Applications, Department of Microsystems Engineering (IMTEK), University of Freiburg, Georges-Koehler-Allee 103, 79110 Freiburg, Germany. E-mail: junichi.miwa@imtek.uni-freiburg.de

sorting method for accurate isolation of a specific cell type from cell mixture will be of great help to reduce the time and cost required.

There are various reports on microscale cell separation based on cell density [7], diameter [8–12] or dielectric properties [13–19]. However, considering the fact that the size of MSC is comparable to certain larger cells in blood (e.g. monocytes) and also that electric fields may affect cell differentiation performance, separation based on these properties is not suitable for rare-cell sorting.

Surface reaction sites such as antigens are promising candidates for cell recognition in rare-cell sorting. Antigens defining MSC are not yet completely determined, but work on clarifying MSC surface markers is underway, together with differentiation schemes into various tissue cells [3–5]. Methods such as fluorescence-activated cell sorting (FACS) [20] or magnetic cell sorting (MACS) [21] are widely accepted both in clinical use and in scientific research, and microfluidic devices capable of cell separation using these principles have been reported [22–30]. These methods require preprocessing of the sample, where antibody-conjugated fluorescent molecules or magnetic microparticles need to be mixed with the sample and attached to the target cells in the suspension. The label molecules or particles should also be removed from the surface of sorted cells prior to transplantation, which requires yet another additional step. These pre- and post-processing procedures required in labelling-based methods make the whole cell separation system quite complicated and costly.

The discussions above show that label-free target cell recognition based on surface antigens is preferable for stem cell extraction. Affinity chromatography is an adhesion-based cell-separation method using an antigen–antibody interaction for target-cell recognition. Antibodies are immobilized on the surfaces of packed particles or microchannels, on which target cells are trapped [31, 32]. Cell separation can be accomplished using a simpler system compared to FACS or MACS but the method bears the difficulty in collecting cells from the device. The same post-processing reagents may be necessary to detach the captured cells from the surface. In order to establish a label-free cell separation method capable of collecting the separated cells without difficulty, devices mimicking leukocyte rolling [33] have been developed, with which separation of leukocytes in a microchannel with selectin-coated pillars has been reported [34].

Recently, Miwa *et al* [35] demonstrated the separation of endothelial cells and leukocytes in an antibody-coated micro column. They employed aminomethyl-functionalized parylene (diX-AM) as the surface material and performed covalent antibody immobilization on the surface amines at extremely high number densities. The antibody-immobilized diX-AM surface functioned as a ‘specifically adhesive surface’, on which a cell type containing the corresponding antigen adheres, while others do not. A mixture of two cell types was introduced into the antibody-immobilized column in the form of a plug, and it was shown that the antibody-specific cells travelling through the column were decelerated by up to 70% compared to the non-specific cells. This resulted

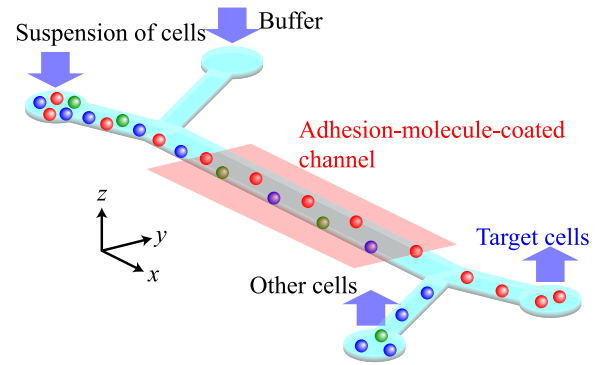


Figure 1. Schematic of the adhesion-based continuous cell separation device.

in streamwise separation of the cell sample, and thus plugs containing each cell type could be separately collected at the outlet. These separation principles are promising in a sense that the demerits of labelling-based methods and previous adhesion-based methods have been overcome. However, because the separation principle is based on cell deceleration, the direction of separation is limited to the streamwise direction. The sample needs to be introduced in the form of a plug of a specified volume in the microchannel. In order to realize a more versatile label-free cell separation platform with flexible capabilities regarding the sample volume or contents, a continuous separation principle should be established.

In the present study, we introduce a novel approach for label-free continuous cell separation in the cross-flow direction according to the antigen expression (figure 1). We design the specifically adhesive surface in such a way that the specific adhesion force induces cross-flow motion of a particular cell type. Sequential asymmetric micropatterns of adhesion molecules are formed on the microchannel wall by uniformly immobilizing streptavidin on the surface of micron-sized oblique grooves that are narrower than the size of a single cell. When the cells reach the boundary between streptavidin-immobilized and non-immobilized regions, the cells shift their position in the cross-flow direction by the asymmetric adhesive force. The consecutive lateral displacement results in cross-flow separation of cell mixture, enabling the sample to be continuously collected at the outlets. We prove our concept of continuous separation with flow-through experiments using different functionalized model particles.

2. Design

Figure 2 shows the schematic of our cross-flow separation principle. The streamwise and cross-flow positions are represented as x and y , respectively. The open circle on the right-hand side represents the area of the cell which is in ‘close contact’ with the specifically adhesive surface. In other words, it corresponds to the area of the cell membrane within a certain distance of the adhesive surface, where attractive force is exerted between the adhesion molecules on the substrate and the cell membrane. The adhesion molecule pattern is inclined at an angle α with respect to the x -direction. The cell is travelling at velocity \mathbf{v} with angular velocity ω . If

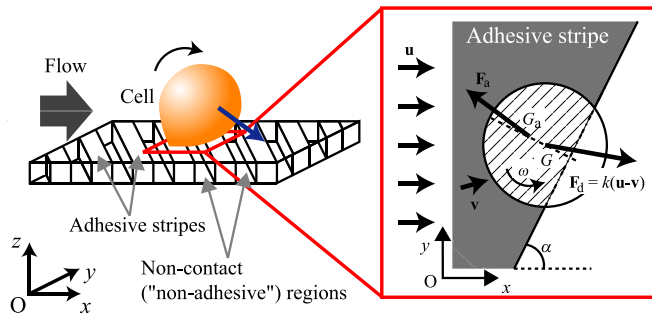


Figure 2. Schematic of the cross-flow motion of cells induced by asymmetry of specific-adhesivity distribution on the surface.

the fluid velocity is uniform in the y -direction, the fluid drag acting on the cell surface (F_d) can be assumed as proportional to the relative velocity of the cell to the flow. The adhesive force F_a acts on the region of the cell membrane where it is in close contact with the surface adhesion molecules, i.e., the area of the open circle that is overlapping with the specifically adhesive region (shaded area in figure 2).

We assume that the adhesive force works in the direction opposite to the local cell membrane motion, and that the integral of the local force distribution acts on the centre of inertia of the overlapping area G_a . When a cell crosses the boundary between surfaces with and without specific adhesivity at a certain angle, the local adhesive force shows an asymmetric distribution in the cross-flow direction. Therefore, the net adhesive force vector F_a points at a certain angle to the flow direction. The sum of two vectors F_d and F_a gives the net force, the cross-flow component of which is non-zero. Non-target cells are not influenced by the adhesive force and thus flow in the direction of the surrounding fluid.

Since the asymmetry of adhesive force distribution occurs only when the cell crosses the border of the specifically adhesive area, the number of oblique stripes should be as large as possible. On the other hand, the force in the cross-flow direction would be cancelled out when the cell membrane is simultaneously in contact with multiple adhesive stripes. Therefore, the stripe width and the gap between adjacent stripes should be larger than the diameter of the contact area.

In the present study, the cell surface is assumed to be in contact with the wall when its distance from the surface is shorter than the bond length of adhesion molecule pairs. Based on the particle diameter of model cells used in our experiments ($7.66 \mu\text{m}$) and the length of an undisturbed selectin bond (20 nm) [36], the streamwise width of the adhesive stripes is determined to be $1 \mu\text{m}$. Stripes of adhesive and non-adhesive regions are realized by fabricating micro-grooves on one of the microchannel walls. The depth of the grooves needs to be as small as possible in order to avoid secondary flow [37], which induces cross-flow motion of both the target and non-target cells. However, cells should not have contact with the bottom surface of the grooves. Based on these requirements, the groove depth is determined as $0.25 \mu\text{m}$.

The microchannel height is chosen as $40 \mu\text{m}$, which is 160 times larger than the groove depth. Therefore, we expect that the effect of local flow inside the grooves on the overall

flow profile is negligible. According to the analytical study by Stroock *et al* [38], the mean slip velocity in the direction of the grooves would be approximately 0.1–0.2% of the channel centre velocity with the geometry described above. The local cross-flow velocity at the wall-normal position $5 \mu\text{m}$ away from the wall can be estimated to be less than 1% of the streamwise velocity. Thus, we expect that the secondary flow caused by the micro-grooves has little effect on the cross-flow motion of the cells. The channel width can be of any dimension as long as the shear rate is not too large, at which shear-induced lift force may become significant. In the present study, the microchannel width is chosen as $200 \mu\text{m}$.

3. Microfabrication

Figure 3 shows the microfabrication process of the cell separation device. A 200 nm thermal oxide layer is formed on both sides of a bare silicon wafer, and a $3.8 \mu\text{m}$ thick photoresist pattern (AZ P4400, AZ Electronic Materials) is made using standard photolithography technique. Using this pattern as the mask, the oxide layer is dry-etched with CHF_3 plasma. After removing the photoresist, the $40 \mu\text{m}$ deep microchannel structure is etched into the silicon substrate using deep reactive ion etching (DRIE) with the Bosch process (Alcatel, AMS-100). Inlet and outlet ports with the diameter of 1 mm are drilled into the silicon substrate using an ultrasonic tool (Cho-onpa Kogyo), and the remaining oxide layer on the patterned side is removed with buffered HF. The backside oxide layer is left for bonding polydimethylsiloxane (PDMS) inlet and outlet ports.

In order to form micro-grooves with the width of $1 \mu\text{m}$ on Pyrex glass wafer, we use electron-beam (EB) lithography. A 250 nm thick layer of positive EB resist (FEP-171, Fuji Film) is spun on the Pyrex glass wafer, and a layer of conductive polymer (Espacer 300AX, Showa Denko) is spun on to prevent the substrate from charging up. The EB exposure is performed using an EB-lithography system (ADV-F5112, Advantest). The photoresist pattern is developed using NMD-3 (2.38% TMAH solution), followed by ICP-RIE (CE-300I, ULVAC) of the glass substrate with CHF_3 plasma. The etch rate is approximately 3 nm s^{-1} , and the selectivity between the EB resist and the Pyrex glass substrate under this condition is approximately 1:1.

After dicing the wafer into $20 \times 20 \text{ mm}^2$ chips, the entire surface of the silicon microchannel structure is coated with a $2 \mu\text{m}$ thick layer of parylene C (diX-C, KISCO) for the thermal bonding process. The backside of the wafer is protected with adhesive tape in order to prevent the oxide layer from being coated. The patterned side of the Pyrex glass wafer is coated with aminomethyl-functionalized parylene (diX-AM, KISCO) with the thickness of $0.1 \mu\text{m}$. Then, the silicon and glass substrates are aligned and thermally bonded to enclose the microchannel structure. The bonding process is performed at a temperature of $150 \text{ }^\circ\text{C}$ under vacuum (in the range of several Pa), while pressing the substrates at the pressure of 5 MPa for 30 min .

PDMS tubing ports are formed with a 6 mm thick PDMS block and by puncturing a 1.5 mm diameter hole. The ports are

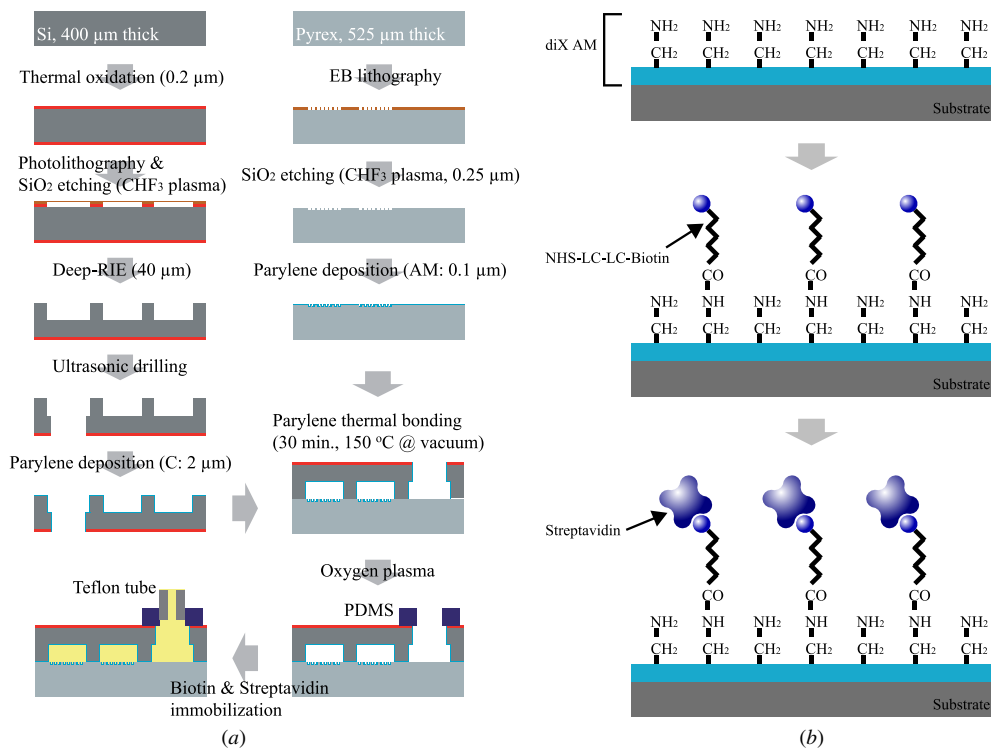


Figure 3. (a) Microfabrication process of the device with micro-grooves for adhesivity pattern formation. (b) Streptavidin immobilization process on diX AM.

attached onto the backside oxide layer of the silicon substrate after treating both the punctured PDMS block and the oxide surface with 26 W oxygen plasma for 20 s. In order to obtain firm bonding, the PDMS-bound chip is loosely clamped and baked at 65 °C in a convection oven.

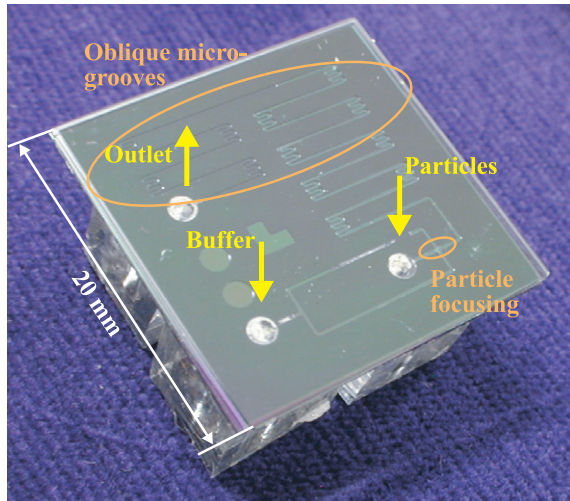
Figure 3(b) shows the schematic of the adhesion molecule immobilization procedure [35]. First, a solution of biotin-NHS ester in DMSO is further dissolved into pH 8 bicine buffer. The solution is introduced into the device and incubated at 30 °C for 1 h. Next, streptavidin is conjugated to the surface-immobilized biotin by incubating the molecules dissolved in phosphate-buffered saline (PBS, pH 7.4). Biotin–streptavidin interaction is used for specific binding in the present study, but the present immobilization scheme is a versatile technique capable of immobilizing any kind of adhesion molecules (e.g. antibodies) on diX-AM via streptavidin, as long as biotinylated chemicals are available.

Figure 4(a) shows the design of the whole separation channel. There are two inlets for particles (cells) and plain buffer and one outlet. The particle stream is hydrodynamically focused by the buffer solution in order to keep the cells in the central part of the channel, where the flow velocity is almost uniform in the cross-flow direction. Micro-grooves forming adhesive stripes (figure 4(b)) are located at the straight parts of the channel, each patterned section being 2 mm long. The total length of the micro-grooved region on the device is 20 mm, which corresponds to 10 000 adhesive stripes. Devices are fabricated with different micro-groove angles varying from 30° to 60°.

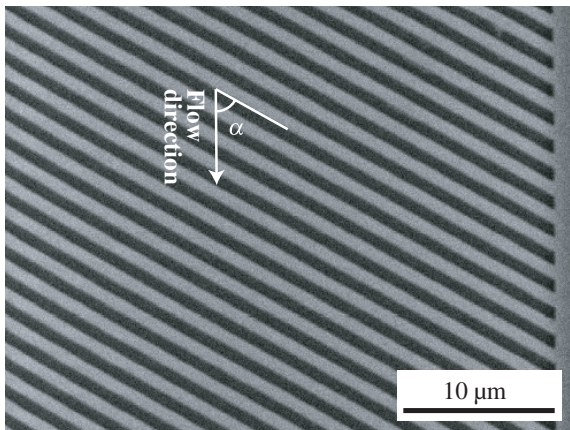
4. Experimental details

As a proof of concept, we have conducted flow-through separation experiments using fluorescent polystyrene particles as substitutes for cells. Biotin-coated yellow polystyrene particles and streptavidin-coated Nile-red particles (Spherotech Inc.) are used to represent the specifically binding and non-binding cells, respectively. The two particles are of the same diameter, with an average of 7.66 μm and a standard deviation of 0.33 μm. The particle concentration is 4.3×10^6 particles mL⁻¹. The specific gravity of the particles is 1.05, which is comparable to white blood cells. Because the only difference between the two particles is the surface chemistry, any difference between the motions of the two particles should be attributed to the difference in adhesivity on the streptavidin-immobilized surface.

The particles are suspended in pH 7.4 PBS, and the same buffer solution is used for hydrodynamic focusing. Sample flow is driven using a syringe pump (CMA Microdialysis, CMA400), which is connected to the PDMS inlet ports with Teflon tubing. The device is placed on an inverted microscope (Olympus, IX-71) with mercury lamp illumination. The emitted fluorescence is filtered using standard filter blocks with a 460–490 nm excitation filter, a 505 nm dichroic mirror and a 510 nm long-pass filter for the biotin-coated yellow particles. For the streptavidin-coated Nile-red particles, a 520–550 nm excitation filter, a 565 nm dichroic mirror and a 580 nm long-pass filter are used. Instantaneous images of flowing particles are captured using a 20× magnification objective with a numerical aperture of 0.75 and a 696 ×



(a)



(b)

Figure 4. Microfabricated cell separation device. (a) Top view of the entire chip and (b) SEM image of the Pyrex glass micro-grooved surface after parylene deposition.

520 pixel Peltier-cooled CCD camera (Qimaging, Rolera-XR) at 25 fps.

Figure 5 shows superimposed sequential instantaneous images of biotin-coated particles flowing in the streptavidin-immobilized channel with $\alpha = 45^\circ$ and $u_b = 0.5 \text{ mm s}^{-1}$. Both the streamwise and cross-flow motion of the particles are derived by measuring the displacement of the particle centre in these sequential images. The particles are spherical and their centre positions could be well defined on the image. We have evaluated the pixel error as ± 1 pixel, which gives a $\pm 0.91 \mu\text{m}$ measurement error for the displacements, given the camera pixel size ($12.9 \mu\text{m}$) and the magnification ($20\times$). The maximum error of streamwise velocity measurements thus estimated is approximately $\pm 0.23 \mu\text{m s}^{-1}$ ($\pm 0.3\%$). The cross-flow displacement rate of particles is defined as the cross-flow displacement Δy divided by the streamwise travelling length Δx , and its measurement error is evaluated as ± 0.0017 . The particle motion is examined at bulk mean velocities (u_b) varying from 0.25 to 1.0 mm s^{-1} , which are determined by the flow rate of sample injection with the syringe pump and the channel dimensions. The corresponding Reynolds number

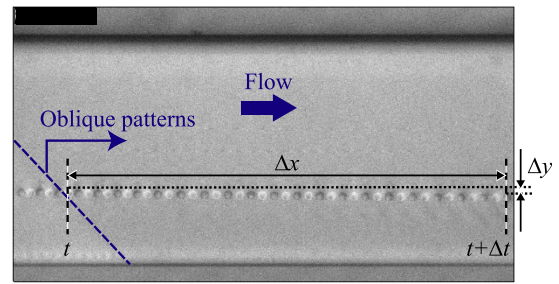
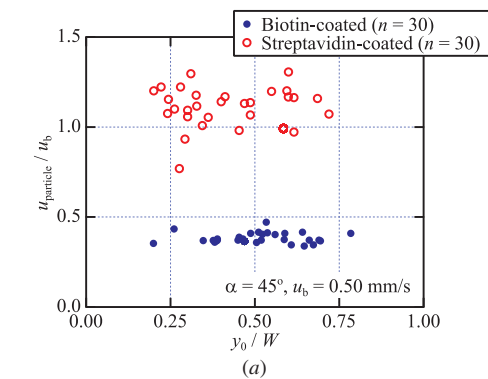
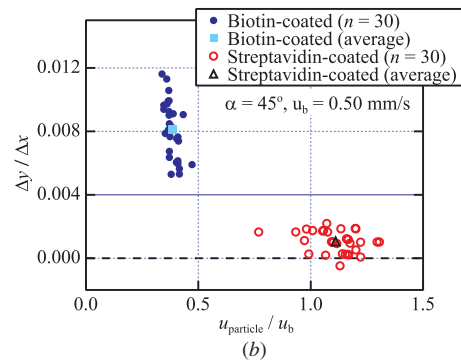


Figure 5. Superimposed instantaneous images of particle motion on the micro-grooved surface. The time increment between each cell position is 40 ms.



(a)



(b)

Figure 6. Motion of particles on the streptavidin-immobilized oblique grooved surface at the first streptavidin-patterned region. (a) Streamwise velocities of individual particles at different cross-flow positions y_0 (normalized by the channel width W) and (b) cross-flow displacement rate $\Delta y / \Delta x$ versus the streamwise velocity. Each data point corresponds to the measurement of a single cell.

($Re = u_b H / \nu$) is 0.008 – 0.03 , where H is the microchannel height ($40 \mu\text{m}$) and ν is the kinematic viscosity of the fluid.

Figure 6(a) shows the variation of the streamwise particle velocity u_{particle} at the first streptavidin-patterned region from the inlet. The motion of 30 individual particles is examined for both biotin- and streptavidin-coated particles. The horizontal axis shows the cross-flow initial particle position y_0 , where the particle enters the streptavidin-patterned region. All the particles within the middle half of the channel are almost uniformly distributed in the cross-flow direction due to the hydrodynamic focusing at the inlet as mentioned above. The velocity of streptavidin-coated particles is slightly higher

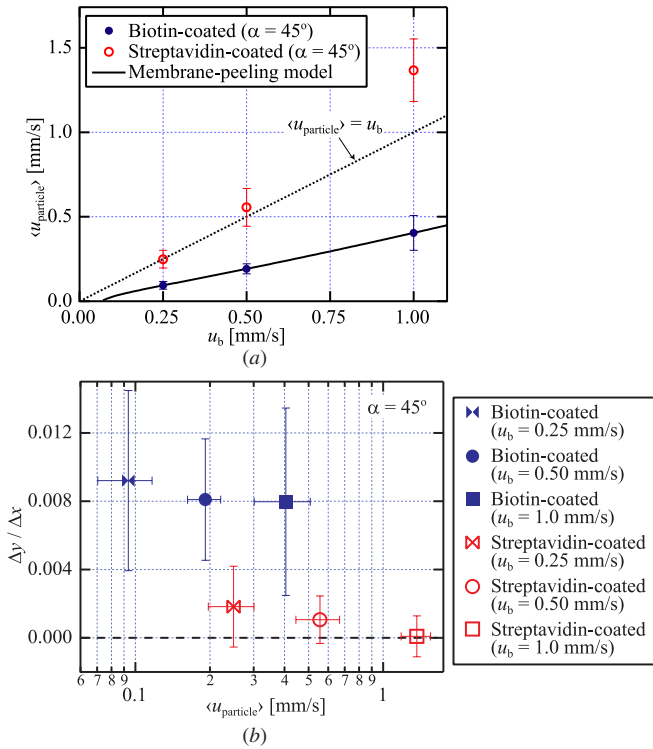


Figure 7. Effect of flow velocity on particle motion. (a) Comparison of the mean streamwise particle velocities $\langle u_{\text{particle}} \rangle$ with membrane-peeling model estimations and (b) comparison between the cross-flow (mean displacement rate $\Delta y / \Delta x$) and streamwise (mean velocity $\langle u_{\text{particle}} \rangle$) motions of the particles. Error bars show twice the standard deviation of data obtained with the 30-cell sample.

than u_b , which indicates that they travel away from the streptavidin-immobilized wall surface. On the other hand, the biotin-coated particles travel at approximately 40% of u_b , regardless of their initial cross-flow positions. Therefore, these ‘adhesive’ particles are captured on the wall by the biotin–streptavidin specific interaction and are rolling at a lower velocity. The cross-flow displacement rate $\Delta y / \Delta x$ for each particle is shown in figure 6(b). Streptavidin-coated (non-adhesive) particles travel almost exactly in the streamwise direction, with $\Delta y / \Delta x$ varying from 0 to 0.002, and its mean value is 0.001. From the aforementioned pixel error, the mean cross-flow displacement of the non-adherent particles can be considered as zero. On the other hand, $\Delta y / \Delta x$ for the biotin-coated particles varies from 0.005 to 0.012 with the average of 0.008. Therefore, the decelerated particles with the specific interaction are significantly displaced in the cross-flow direction on the streptavidin-patterned surface.

In order to investigate the effect of flow velocity on the motion of adherent particles, experiments at varying flow velocity are performed in a streptavidin-immobilized channel with $\alpha = 45^\circ$. Figure 7(a) shows the ensemble-averaged velocities of biotin- and streptavidin-coated particles $\langle u_{\text{particle}} \rangle$ at the upstream-most streptavidin-coated region. Velocities of 30 individual particles are measured for each particle type. In all cases examined, mean velocities of the streptavidin-coated particles are equal to or larger than u_b . On the other hand, the adhesive biotin-coated particles are decelerated by

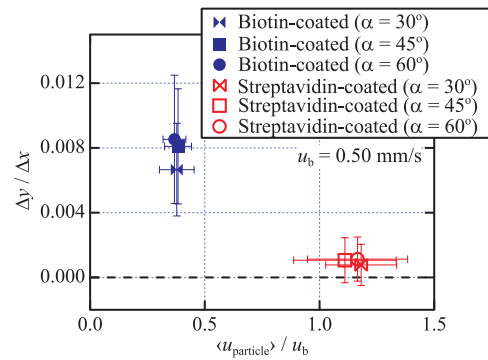


Figure 8. Mean cross-flow displacement versus mean streamwise velocity for different streptavidin pattern angles at $u_b = 0.50 \text{ mm s}^{-1}$. Error bars show twice the standard deviation.

approximately 40% in all three cases. The trend of particle deceleration is compared with the estimates based on the semi-analytical membrane-peeling model developed by Dembo *et al* [39]. The model parameters are determined by a curve fitting to the experimental data using the least-square method. The biotin-coated particles show very good accordance with the model, confirming that the deceleration is caused by the specific interaction between the surface and particles. Interestingly, the deceleration rate of biotin-coated particles observed here is comparable to that of human umbilical-vein endothelial cells (HUVEC) in a CD31-antibody immobilized microchannel [35], despite the difference in the on-rates and off-rates of the different binding molecules.

The mean cross-flow displacements of the particles for different flow velocity are shown in figure 7(b). The cross-flow displacement rates of biotin-coated particles are independent of u_b , with $\Delta y / \Delta x \sim 0.8$ for all the cases examined. Although $\Delta y / \Delta x$ of streptavidin-coated particles are somewhat scattered at the lowest flow rate condition, there is a clear difference between the cross-flow motion of adherent and non-adherent particles. Because the difference in $\Delta y / \Delta x$ between the two particle types increases at higher flow rates, it is conjectured that cross-flow separation is possible at much higher flow velocities, which leads to higher throughput of the device.

Figure 8 shows the mean particle velocities and their cross-flow displacements for different angles of the streptavidin pattern at $u_b = 0.50 \text{ mm s}^{-1}$. It is found that the cross-flow displacements of biotin-coated particles are unchanged for different α , and $\Delta y / \Delta x$ remains at about 0.008. On the other hand, the cross-flow displacements of streptavidin-coated particles are within the uncertainty of the present measurements and negligibly small. Recently, Karnik *et al* [40] performed experiments with HL-60 cells in a microchannel with *p*-selectin patterning with a single border between adhesive and non-adhesive regions. They report that the rolling of cells was only observed at smaller angles (10–15° or less), at which cells intermittently stopped and started rolling again at the border of the adhesive region. Since the *p*-selectin pattern has only a single border, the cells are no longer affected by the lateral adhesive force when they have completely escaped from the adhesive region. On the other hand, in the present study, adherent particles are slightly

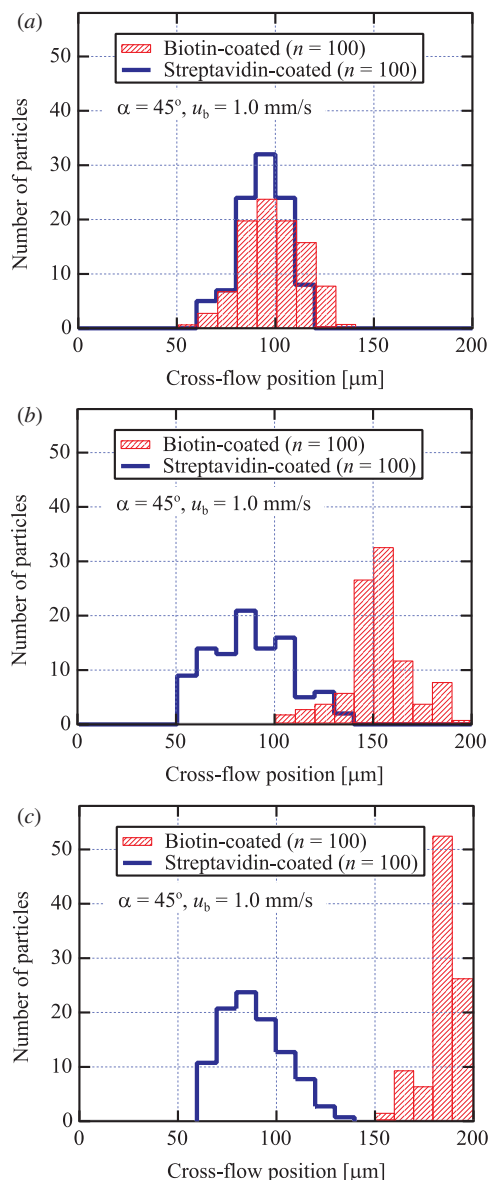


Figure 9. Histograms of the cross-flow positions of particles for $u_b = 1.0 \text{ mm s}^{-1}$ and $\alpha = 45^\circ$. Biotin- and streptavidin-coated particles are separately introduced into the channel. (a) At the inlet of the first streptavidin-patterned section, (b) after passing 10 mm of streptavidin-patterned region and (c) at the outlet of the final streptavidin-patterned section.

deflected each time they pass the streptavidin-immobilized stripes, and the consecutive passage of the particles over multiple stripes makes the particle deflection significant. In the following section, experiments are performed at $u_b = 1.0 \text{ mm s}^{-1}$ and $\alpha = 45^\circ$.

Figure 9 shows the cross-flow distributions of biotin- and streptavidin-coated particles at different streamwise measurement stations. As described earlier, the uncertainty of particle position measurement is $\pm 0.91 \mu\text{m}$. In this experiment, the particles are separately introduced into the device, and the positions of 100 particles are investigated. Near the inlet, both types of particles are confined within the middle $100 \mu\text{m}$ of the channel. After passing 10 mm of the streptavidin-patterned region (5000 adhesive stripes),

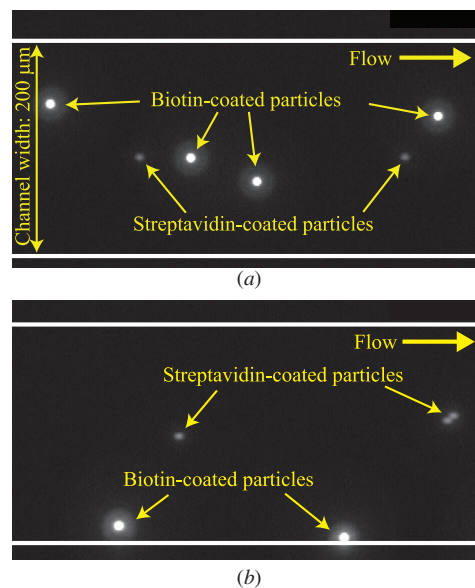


Figure 10. Snapshots of biotin- and streptavidin-coated particles on the streptavidin-immobilized surface. (a) Inlet of the first streptavidin-patterned section and (b) outlet of the final streptavidin-patterned section.

the distribution of biotin-coated particles is significantly displaced in the cross-flow direction. At the exit of the last patterned section, which corresponds to 20 mm of the streptavidin-patterned region (10 000 adhesive stripes), biotin-coated particles are all concentrated close to the sidewall, while the streptavidin-coated particles are located in the middle of the channel.

It is now clearly shown that particles with specific adhesivity to surface-patterned adhesion molecules can be significantly displaced in the cross-flow direction. Finally, we demonstrate the effectiveness of our device in separating a mixture of particles with different surface functionalization. A mixture of biotin-coated yellow and streptavidin-coated Nile-red particles is introduced into the streptavidin-immobilized channel. We use the optical filter set for observing yellow particles (460–490 nm excitation filter and 510 nm long-pass filter). The excitation wavelengths for the two particles partially overlap, enabling the two particles to be simultaneously visualized and distinguished based on their fluorescence intensities. In order to avoid specific binding between the biotin- and streptavidin-coated particles, we blocked the surface of streptavidin-coated particles with a human biotin-conjugated CD15 antibody (eBioscience Inc.). With this surface blocking, we have not observed any agglomeration of particles in the actual flow-through experiments.

Figure 10 shows snapshots of particles close to the inlet (figure 10(a)) and the outlet (figure 10(b)). It can be clearly seen that the particles are located in the centre part of the channel at the inlet, and biotin-coated particles shift to the sidewall at the outlet. The streptavidin-coated particles remain in the middle of the channel, resulting in successful separation of the specific and non-specific particles. Note that although the particles have the same diameters of $7.66 \mu\text{m}$, biotin-coated particles appear larger in the images due to their higher

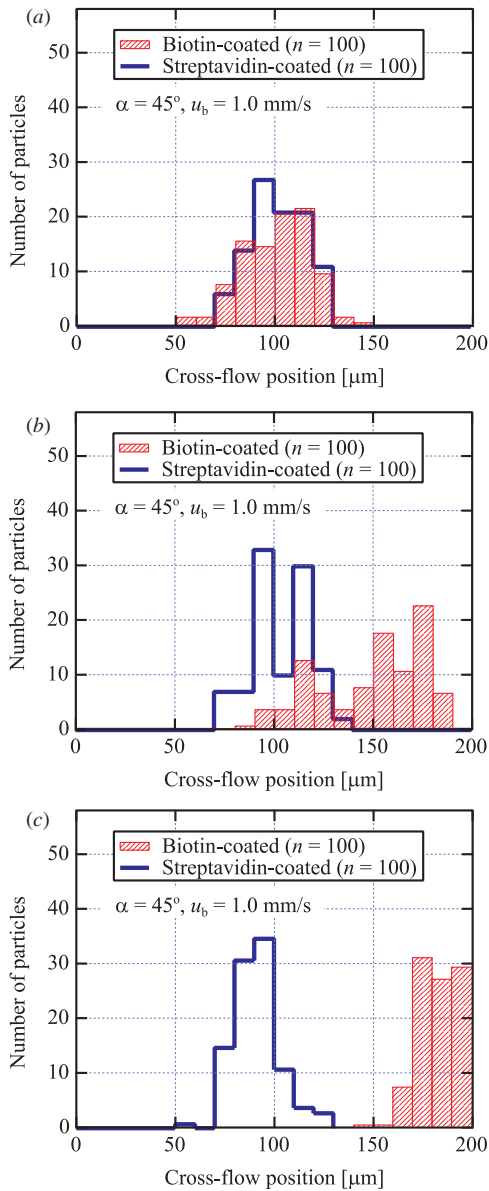


Figure 11. Histograms of the cross-flow positions of particles for $u_b = 1.0 \text{ mm s}^{-1}$ and $\alpha = 45^\circ$. Mixture of biotin- and streptavidin-coated particles is introduced into the channel. (a) At the inlet of the first streptavidin-patterned section, (b) after passing 10 mm of streptavidin-patterned region and (c) at the outlet of the final streptavidin-patterned section.

image intensity. Figure 11 shows histograms of the cross-flow positions of the particles. As in the previous experiments shown in figure 9, all particles are concentrated in the middle $100 \mu\text{m}$ of the channel at the first patterned section. As the biotin-coated particles flow downstream, they are displaced towards the sidewall downstream. At the final patterned section, there is no overlap of the particle distribution of different types, which demonstrates that adherent particles can be completely separated from the non-adherent particles within the 20 mm length. While the particles were distributed in the middle $100 \mu\text{m}$ region of the channel at the inlet, biotin particles were concentrated in the region within $50 \mu\text{m}$ from the sidewall after passing the streptavidin-patterned

regions. This indicates that the specific target is not only separated but also enriched by a factor of 2 using the present separation device. We expect that larger enrichment can be achieved simply by increasing the number of patterns on the channel.

In the present study, the proof-of-concept experiments were performed using surface-functionalized polystyrene particles as model cells. Although the association constant or binding strength of streptavidin/biotin bonds is significantly larger compared to those of antigen/antibody bonds, the rates of particle deceleration (figure 7(a)) are very similar to what was observed with HUVEC in a microchannel with a uniformly immobilized CD31 antibody [35]. Therefore, we expect the same order of cross-flow displacement and thus successful separation with cells and surface-immobilized antibodies in the present device. In some applications, the cell size may be different from the model particles used in the present study. Considering that the fluid drag and adhesive force are respectively proportional to the cell diameter and the cell diameter squared, we can expect that the smaller the target cell, the relatively weaker the effect of cross-flow displacement. On the other hand, smaller cell diameters allow narrower adhesive stripes and thus more frequent occasions of cross-flow displacement since the displacement should occur at the border between adhesive and non-adhesive regions. The balance between these two effects is an interesting issue that should be investigated in the future.

The throughput of the present separation device is approximately $70 \text{ particles s}^{-1}$, which is two orders of magnitude less compared to conventional FACS. We consider that this is primarily due to the low particle concentration, and we expect further improvements in throughput to be made by simply increasing the sample particle concentration and possibly the sample flow rate. According to experimental and numerical investigations on the particle–particle (cell–cell) interactions in adhesion-mediated rolling [41], the particle–particle interaction induces significant changes in the rolling velocity when the distance between particles is smaller than approximately three times the particle diameter at the shear rate of 80 s^{-1} . The shear rate is on the same order as in our current study, and the distance between particles corresponds to the cell concentration in the range of 10^8 – $10^9 \text{ cells mL}^{-1}$, which leaves room for a 1000-fold increase from our current conditions.

5. Conclusions

We have proposed a label-free continuous adhesion-based cell separation method using oblique adhesion molecule patterns, for the separation of rare cells which could only be detected via surface markers. The specifically adhesive pattern is formed on the microchannel wall by uniformly immobilizing streptavidin on $1 \mu\text{m}$ wide, $0.25 \mu\text{m}$ deep micro-grooves, which are inclined to the streamwise direction. When the cell crosses the border between streptavidin-immobilized and non-immobilized regions, the adhesive force induces cross-flow movement due to asymmetry of the specific adhesivity distribution.

We evaluate the performance of the present device by flow-through experiments using 7.66 μm polystyrene particles with biotin- or streptavidin-coating in a microchannel with a streptavidin-immobilized wall. The following conclusions have been derived.

- Particles influenced by specific adhesion are significantly shifted in the cross-flow direction, while no cross-flow motion is observed for the non-specific particles.
- Cross-flow displacement rates as large as 0.8% are observed for the adherent particles. Parameters such as the flow velocity and groove angle had little influence on this cross-flow displacement rate in the range investigated here.
- A mixture of streptavidin- and biotin-coated particles is successfully separated in the cross-flow direction using the present device.

The adhesion molecule immobilization scheme used in the present study is a highly versatile method which easily enables antibody immobilization on a vast variety of surfaces [35]. Regarding the promising results we have obtained using functionalized polystyrene particles of the same diameter as typical white blood cells, we believe our present method should be successfully applicable to the separation of biological cells. Also cell sorting with multiple antigen-antibody interactions could be easily realized by immobilizing several different antibodies on the micro-groove surface, and/or serially connecting separation components with different antibody immobilizations.

Acknowledgments

We thank Professors T Ushida and K Furukawa of the University of Tokyo for the preparation of cell samples. The present work was supported through Grant-in-Aid for Scientific Research (S) (no 15106004) by MEXT, Japan. The photomasks for photolithography and the micro-grooves on Pyrex glass were fabricated using the direct EB lithography system (ADV-F5112, ADVANTEST) of VLSI Design and Education Center (VDEC) in the University of Tokyo.

References

- [1] Evans M J and Kaufman M H 1981 Establishment in culture of pluripotential cells from mouse embryos *Nature* **225** 154–6
- [2] Takahashi K and Yamanaka S 2006 Induction of pluripotent stem cells from mouse embryonic and adult fibroblast cultures by defined factors *Cell* **126** 663–76
- [3] Jiang Y *et al* 2006 Pluripotency of mesenchymal stem cells derived from adult marrow *Nature* **418** 41–9
- [4] Bieback K, Kern S, Klüter H and Eichler H 2004 Critical parameters for the isolation of mesenchymal stem cells from umbilical cord blood *Stem Cells* **22** 625–34
- [5] Lee O K, Kuo T K, Chen W-M, Lee K-D, Hsieh S-L and Chen T-H 2004 Isolation of multipotent mesenchymal stem cells from umbilical cord blood *Blood* **103** 1669–75
- [6] Krause D S, Theise N D, Collector M I, Henegariu O, Hwang S, Gardner R, Neutzel S and Sharkis S J 2001 Multi-organ, multi-lineage engraftment by a single bone marrow-derived stem cell *Cell* **105** 369–77
- [7] Hsu C-H, Carlo D D, Chen C, Irimia D and Toner M 2008 Microvortex for focusing, guiding and sorting of particles *Lab Chip* **8** 2128–34
- [8] Yamada M and Seki M 2004 Microfluidic particle sorter employing flow splitting and recombining *Anal. Chem.* **78** 1357–62
- [9] Zheng S J, Liu J-Q and Tai Y-C 2008 Streamline-based microfluidic devices for erythrocytes and leukocytes separation *J. Microelectromech. Syst.* **17** 1029–38
- [10] Bhagat A A S, Kuntaegowdanahalli S S and Papautsky I 2008 Continuous particle separation in spiral microchannels using dean flows and differential migration *Lab Chip* **8** 1906–14
- [11] Choi S and Park J-K 2007 Continuous hydrophoretic separation and sizing of microparticles using slanted obstacles in a microchannel *Lab Chip* **7** 890–7
- [12] Morton K J, Louterback K, Inglis D W, Tsui O K, Sturm J C, Chou S Y and Austin R H 2008 Crossing microfluidic streamlines to lyse, label and wash cells *Lab Chip* **8** 1448–53
- [13] Voldman J 2006 Electrical forces for microscale cell manipulation *Ann. Rev. Biomed. Eng.* **8** 425–54
- [14] Marx G H, Rousselet J and Pethig R 1997 DEP-FFF: field-flow fractionation using non-uniform electric fields *J. Liq. Chromatogr. Relat. Technol.* **20** 2857–72
- [15] Yang J, Huang Y, Wang X, Wang X-X, Becker F F and Gascoyne P R C 1999 Dielectric properties of human leukocyte subpopulations determined by electrorotation as a cell separation criterion *Biophys. J.* **76** 3307–14
- [16] Rosenthal A and Voldman J 2005 Dielectrophoretic traps for single-particle patterning *Biophys. J.* **88** 2193–205
- [17] Ohta A T, Chiou P-Y, Han T H, Liao J C, Bhardwaj U, McCabe E R B, Yu F, Sun R and Wu M C 2007 Dynamic cell and microparticle control via optoelectronic tweezers *J. Microelectromech. Syst.* **16** 491–9
- [18] Tai C-H, Hsiung S-K, Chen C-Y, Tsai M-L and Lee G-B 2007 Automatic platform for cell separation and nucleus collection *Biomed. Microdev.* **9** 533–43
- [19] Chang S and Cho Y-H 2008 A continuous size-dependent particle separator using a negative dielectrophoretic virtual pillar array *Lab Chip* **8** 1930–6
- [20] Bonner W A, Hulett H R, Sweet R G and Heizenberg L A 1972 Fluorescence activated cell sorting *Rev. Sci. Instrum.* **43** 404–9
- [21] Douglas G C and King B F 1989 Isolation of pure villous cytotrophoblast from term human placenta using immunomagnetic microspheres *J. Immunol. Methods* **119** 259–68
- [22] Fu A Y, Spence C, Scherer A, Arnold F H and Quake S R 1999 A microfabricated fluorescence-activated cell sorter *Nat. Biotechnol.* **17** 1109–11
- [23] Takahashi K, Hattori A, Suzuki I, Ichiki T and Yasuda K 2004 Non-destructive on-chip cell sorting system with real-time microscopic image processing *J. Nanobiotechnol.* **2** 5
- [24] Berger M, Castelino J, Huang R, Shah M and Austin R H 2001 Design of a microfabricated magnetic cell separator *Electrophoresis* **22** 3883–92
- [25] Pamme N and Manz A 2004 On-chip free-flow magnetophoresis: continuous flow separation of magnetic particles and agglomerates *Anal. Chem.* **76** 7250–6
- [26] Tan W-H, Suzuki Y, Kasagi N, Shikazono N, Furukawa K and Ushida T 2005 A lamination micro mixer for μ -immunomagnetic cell sorter *JSME Int. J. Ser. C* **48** 425–35
- [27] Han K-H and Frazier A B 2006 Paramagnetic capture mode magnetophoretic microseparator for high efficiency blood cell separations *Lab Chip* **6** 265–73

- [28] Inglis D W, Riehn R, Sturm J C and Austin R H 2006 Microfluidic high gradient magnetic cell separation *J. Appl. Phys.* **99** 08K101
- [29] Inokuchi H, Suzuki Y and Kasagi N 2008 Development of micro immuno-magnetic cell sorting system with lamination mixer and magnetic separator *Proc. 25th Sensor Symp. (Okinawa, Japan, 2008)* pp 851–2
- [30] Saias L, Saliba A-E, Pierga J-Y, Vielh P, Farace F and Viovy J-L 2008 Microfluidic magnetic cell sorting system for cancer diagnosis *Proc. 12th Int. Conf. Miniaturized Systems for Chem. and Life Sci. (μ TAS)* pp 552–4
- [31] Ujam L B, Clemmitt R H, Clarke S A, Brook R A, Rushton N and Chase H A 2003 Isolation of monocytes from human peripheral blood using immuno-affinity expanded-bed adsorption *Biotechnol. Bioeng.* **83** 554–66
- [32] Sin A, Murthy S K, Revzin A, Tompkins R G and Toner M 2005 Enrichment using antibody-coated microfluidic chambers in shear flow: model mixtures of human lymphocytes *Biotechnol. Bioeng.* **91** 816–26
- [33] Atherton A and Born G V R 1973 Relationship between the velocity of rolling granulocytes and that of the blood flow in venules *J. Physiol.* **233** 157–65
- [34] Chang W C, Lee L P and Liepmann D 2005 Biomimetic technique for adhesion-based collection and separation of cells in a microfluidic channel *Lab Chip* **5** 64–73
- [35] Miwa J, Suzuki Y and Kasagi N 2008 Adhesion-based cell sorter with antibody-coated amino-functionalized-parylene surface *J. Microelectromech. Syst.* **17** 611–22
- [36] Bell G I, Dembo M and Bongrand P 1984 Cell adhesion—competition between non-specific repulsion and specific binding *Biophys. J.* **45** 1051–64
- [37] Stroock A D, Dertinger S K W, Ajdari A, Mezic I, Stone H A and Whitesides G M 2002 Chaotic mixer for microchannels *Science* **295** 647–51
- [38] Stroock A D, Dertinger S K, Whitesides G M and Ajdari A 2002 Patterning flows using grooved surfaces *Anal. Chem.* **74** 5306–12
- [39] Dembo M, Torney D C, Saxman K and Hammer D 1988 The reaction-limited kinetics of membrane-to-surface adhesion and detachment *Proc. R. Soc. B* **234** 55–83
- [40] Karnik R, Hong S, Zhang H, Mei Y, Anderson D G, Karp J M and Langer R 2008 Nanomechanical control of cell rolling in two dimensions through surface patterning of receptors *Nano Lett.* **8** 1153–8
- [41] King M R and Hammer D A 2001 Multiparticle adhesive dynamics. Interaction between stably rolling cells *Biophys. J.* **81** 799–813